X-621-72-260

PREPRINT

NASA TM X- 65978

THE EQUATORIAL AIRGLOW AND THE IONOSPHERIC GEOMAGNETIC ANOMALY

ORIGINAL CONTAINS COLOR ILLUSTRATIONS

S. CHANDRA
E. I. REED
B. E. TROY, JR.
J. E. BLAMONT

AUGUST 1972

GODDARD SPACE FLIGHT CENTER
GREENBELT, MARYLAND

THE EQUATORIAL AIRGLOW AND THE IONOSPHERIC GEOMAGNETIC ANOMALY

by

S. Chandra, E. I. Reed, B. E. Troy, Jr.
Laboratory for Planetary Atmospheres
Goddard Space Flight Center
Greenbelt, Maryland 20771

and

Jacques E. Blamont
Service d'Aéronomie
Centre National de la Recherche Scientifique
Boite Postale No. 3
91 – Verrières le Buisson
France

THE EQUATORIAL AIRGLOW AND THE IONOSPHERIC GEOMAGNETIC ANOMALY

ABSTRACT

OGO-4 observations of OI (6300Å) emissions have revealed a global pattern in the equatorial airglow hitherto undetected from the ground based observations. It is seen that the post-sunset emission rate of OI (6300Å) is generally very asymmetrical with respect to the geomagnetic equator and shows no apparent correlation with the ultraviolet airglow (OI 1304 and1356Å) and F-region electron density measured simultaneously from the same spacecraft. Both the ultraviolet airglow and the ion density measured in the altitude region of 450 km follow similar latitudinal variations and exhibit the well known properties of the equatorial ionospheric anomaly. The asymmetry in the OI (6300Å) emission can be attributed to the asymmetry in the height of the F-2 maximum as inferred from the height of the maximum emission. From correlative studies of the airglow and the ionospheric measurements, the mechanisms for the ultraviolet and the 6300°A emission are discussed in terms of the processes involving radiative and dissociative recombinations. A relationship between molecular oxygen density and the integrated OI (6300Å) emission rate is derived and the feasibility of using this relationship for estimating O_2 density is discussed.

THE EQUATORIAL AIRGLOW AND THE IONOSPHERIC GEOMAGNETIC ANOMALY

INTRODUCTION

The existence of the tropical arcs was first noted by Barbier and Glaume (1960) from ground based scanning photometers at Tamanrasset (Algeria). Their observations revealed that the 6300Å emission was very often in the form of an east-west arc usually moving from north to south during the course of the night. The extension of these observations to lower latitudes revealed a rather striking similarity between the OI (6300Å) emission and F-region equatorial anomaly in electron density (Barbier, Weil and Glaume, 1961; Barbier and Glaume, 1962). The emission intensity of OI (6300Å) and F-region critical frequency followed a similar latitudinal pattern; i.e., they both had their minimum values at the equator and their maximum values at about 15°-20° on either side of the geomagnetic equator. The observational data which formed the basis of this conclusion was largely obtained from the African longitudes and was very limited at best. Notwithstanding, the success of the Barbier formula relating the 6300Å zenith intensity to the F-region critical frequency and virtual height led to the general belief that the intertropical arcs were of global character and they were the manifestations of the same phenomena which gave rise to the geomagnetic anomaly.

These generalizations could not be verified in detail because of the lack of observing stations in various longitude zones, particularly in the southern latitudes,

but a difficulty became apparent when the observational data from different stations in the African and Pacific zones were compared. King (1968) using the airglow data obtained from the scanning photometers at Tamanrasset (22.8°N, 5.5°E) and Agadez (17.0°N and 8.0°E) deduced the rate of the movement of the arcs towards the equator and found it to be similar to the rate of the movement of the crests of the electron density. VanZandt and Peterson (1969) using the observational data from Maui (20.7°N and 156.3W) obtained a much more complex picture of the equatorial airglow than one would infer from the variations of critical frequency. They concluded that movement of the F-layer, rather than the vertical changes in electron density, is the controlling factor in determining the morphology of the equatorial airglow.

In recent years, the nature of the intertropical arcs has also been studied in the ultraviolet region (Hicks and Chubb, 1970; Barth and Schaffner, 1970), particularly the OI lines at 1304 and 1356Å, and this has added a new dimension to the study of the equatorial airglow. A number of suggestions have been made for the possible origin of the ultraviolet airglow in the equatorial region, ranging from the chemical processes involving radiative recombination to the direct excitation of atomic oxygen by the precipitating energetic particles (Hanson, 1969; Hicks and Chubb, 1970; Barth and Schaffner, 1970; Knudsen, 1970; Olson, Peterson and Mosley, 1971; Zipf and Stone, 1971).

The OGO-4 satellite has provided a unique opportunity to study the nature of the equatorial airglow since the airglow measurements both in the visible and the ultraviolet region were made almost simultaneously with the measurement

of a number of ionospheric parameters needed for the understanding of the possible physical mechanisms. The purpose of this paper is to present a detailed global picture of the equatorial airglow as obtained from the OGO-4 satellite and discuss its characteristics in relation to the ionospheric data obtained from the same spacecraft.

Instrumentation

The OGO-4 satellite was an attitude-stabilized polar orbiting observatory covering an altitude range of 400-900 km. The 6300Å airglow measurements were made using photometers located on the main body and on the OPEP (Orbital Plane Experiment Package). The main body photometer was designed to measure the integrated vertical emission below the spacecraft. The OPEP photometer, through its scan across the horizon, was capable of measuring the vertical airglow profiles (Reed & Blamont, 1967, 1972). The ultraviolet photometers consisted of gas photoionization chambers sensitive in various regions between 1000Å and 1600Å. These emissions were identified as 1304Å and 1356Å lines of atomic oxygen as a result of simultaneous observations by an ultraviolet spectrometer, also on OGO-4. (Hicks and Chubb, 1970; Barth and Schaffner, 1970). The retarding potential analyzer aboard the same spacecraft was designed to make in-situ measurements of electron and ion temperatures, ion composition, and the flux of suprathermal electrons (Chandra, Troy, Donley and Bourdeau, 1970).

In late October, 1967, the perigee of the satellite (418 km) was near the equator at a local time of about 2130. This is also the altitude region of the F_2 peak in the equatorial region. This condition, therefore, permitted the most meaningful comparison of the equatorial airglow and the plasma density.

Discussion of Observational Data

Figure 1 is a contour map of the integrated emission rate of 6300Å airglow constructed from the observational data obtained between October 26-30, 1967, corresponding approximately to the post-sunset condition. The abscissa and the ordinate represent the geodetic longitude and latitude, and the heavy black line corresponds to the position of the magnetic dip equator. This local time (2146) shown on this map is a nominal local time. All points on this map were obtained within 20 minutes of this time, the differences being due to the inclination of the orbit, the range in latitude, and the movement of the plane of the orbit. Because of the large variation in the column emission rate ranging from less than 25 rayleighs to values exceedings 800 rayleighs, the map was constructed by choosing the contours at logarithmic intervals. Also plotted in this map are the positions of the maximum intensity of ultraviolet airglow (heavy dots) as simultaneously observed by Hicks and Chubb (1970). For the purpose of discussion we may divide the map into three zones centered around -75°, 0, and 120° longitudes. These regions are generally referred to as American, African and Asian zones. The general features of this map concerning the nature of the equatorial airglow may be summarized as follows:

1. The global distribution of 6300Å airglow intensity is very asymmetrical with respect to the geomagnetic equator over a wide longitude zone. During the post-sunset condition when the northern arc has covered the entire globe parallel to the geomagnetic equator, the southern arc is present only in the African zone and is almost absent in the American and Asian zones.

2. There is no indication of this asymmetry in the ultraviolet airglow. The positions of the UV intensity maxima (heavy dots) are uniformly distributed in

all the longitude zones and are symmetrical with respect to the geomagnetic equator. In the American and Asian zones the difference between the latitudinal characteristics of the ultraviolet and 6300Å airglow is particularly noticeable The 6300Å arc is absent in the southern latitudes. These observations indicate that although similarities can be inferred between the nature of the tropical arcs of 6300Å airglow and of ultraviolet airglow, their emissions are controlled by different processes.

Figure 2 shows the variations of 6300Å emission rate and O^+ density for three selected orbits in the Asian, American and African zones. The local time for this measurement is about 2130. The altitude of the satellite, which is also the altitude at which O^+ is measured, is shown along with the geomagnetic latitude. The O^+ variations in this figure show the well known features of the geomagnetic anomaly in all the three zones. The density increases continuously on either side of the geomagnetic equator, attains maximum values at about ±20° latitude and then drops off towards mid-latitudes. General resemblances between the latitudinal variations of 6300Å airglow and O^+ density can be inferred only from the African zone. Both the Asian and American zones show a highly asymmetrical variation of 6300Å and a clear maximum is indicated only in the northern zone. In the American zones, the differences in the behavior of 6300Å airglow and O^+ are much more evident in the southern latitudes. When we compare the O^+ variations with the ultraviolet airglow variations (not shown), we find much better correlations in all the longitude zones and almost one-to-one correspondence between the crest of the geomagnetic anomaly and the position of the UV arc. We may, therefore, conclude from these observations that the equatorial

ionospheric anomaly is much better manifested in the tropical UV arcs than in the tropical red arcs. It is interesting to note that ultraviolet airglow observations are very recent. The relationship between the red tropical arcs and the geomagnetic anomaly has been discussed for almost a decade and was based primarily on observational data from the African zone where the 6300Å airglow follows the variations of O^+ rather remarkably well.

Both the 6300Å and the ultraviolet airglow emission may be caused either by chemical recombination involving molecular and atomic oxygen ions or by direct excitations of atomic oxygen by precipaitating particles of different energy ranges. The 6300Å emission may also be caused by thermal excitations of atomic oxygen by electrons at high temperatures. The simultaneous measurement of these parameters from OGO-4 was useful in choosing among these various alternatives. Figure 3 is a typical example of the measurement of the electron and ion temperatures (T_e, T_+) and flux of the suprathermal electrons. The plot in this figure corresponds to a pass in the Asian zone where we have noted considerable asymmetry in the 6300Å airglow. Figure 3 shows that the variations of both T_e and T_+ are relatively small in the equatorial region and their values are usually less than 1600°K. In this temperature range, any contribution to the 6300Å emission caused by thermal excitation is almost negligible. The latitudinal variations of the suprathermal electrons also do not show any pattern which can be associated with the latitudinal variations of either 6300Å or ultraviolet airglow. In order to explain the observed ultraviolet airglow emission by suprathermal electrons, it is necessary to have electron fluxes of the order $10^9/cm^2$-sec in the energy range of 10-20 eV. Our observations,

therefore, tend to reject the concept that the suprathermal electrons play an appreciable role in causing the ultraviolet airglow in the equatorial region. A close correlation between the variations of O^+ ions and ultraviolet airglow, on the other hand, tends to favor the radiative recombination of electrons and ions as a possible mechanism, at least qualitatively (Hanson, 1969).

The lack of correlation between O^+ and 6300Å in certain longitude zones is not at all surprising once we compare the altitude profiles of the 6300Å emission rate in the various longitude zones. In general, there is an inverse correlation between the integrated emission rate and the altitude of the maximum emission. In Figure 4, we have shown the relative variations of the two parameters for the three zones. The integrated emission rate has been obtained from the main body photometer, as in Figure 1 and 2, and the altitude of the maximum emission rate has been estimated from the scanning photometer. In our representation, we have distinguished the observational data points from the northern and southern latitudes by crosses and circles. The main points to be noted from Figure 4 are as follows:

1. The altitude of the maximum emission varies from about 250-350 km in both the Asian and American zones. In the African zone this range is mostly between 250-300 km.

2. The altitude of the maximum is higher in the southern latitudes in both the Asian and American zones. In the African zones there is no noticeable asymmetry.

3. In both the Asian and American zones, the relationship between integrated emission rate, I_{6300} (zenith), and the altitude of the maximum, z (I max), is approximately

$$\log I = -\frac{z}{H}(I \max) + \text{constant} \qquad (1)$$

where H is in the range of 40-45 km. If we identify H with the scale height of molecular oxygen, we may infer a neutral temperature T_n, in the range of 1300-1400°K from the relation $H = kT/M(O_2)g$ with k as Boltzmann constant, $M(O_2)$, the mean molecular mass of O_2, and g, the acceleration due to gravity. This temperature is characteristic of the high solar flux measured during this period and is in reasonable agreement with the neutral temperature inferred from the measurement of the ion temperature T_+ (Fig. 3), which is typically in the range of 1400-1500°K. A difference of about 100°K between T_+ and T_n is to be expected due to the neutral wind heating of the ions (Stubbe and Chandra, 1971).

Theoretical Discussion

The relationship between the integrated emission rate and the height of the peak emission discussed in the previous section is a direct consequence of the dissociative recombination of O_2^+ and electrons. Thus the longitudinal asymmetry of 6300Å airglow and its lack of correlation with electron and ion density merely reflect the zonal asymmetry in the variation of the F_2 peak. The physical processes affecting the F_2 peak are (1) plasma diffusion, (2) electric fields, and (3) neutral winds associated with the meridional and zonal pressure gradients.

These processes are usually not independent of each other and have a large number of geophysical parameters in common. The theoretical description of these processes, therefore, depends upon solving a large number of basic ionospheric and atmospheric equations involving time dependent equations of continuity, momentum and energy balance. The understanding of the longitudinal

asymmetry, in addition, would require a three dimensional solution of this problem taking into account the variations of the geomagnetic field with respect to the geographic coordinates. Notwithstanding the mathematical and numerical complexity in obtaining such solutions, we may understand the nature of the basic physical processes influencing the characteristics of the equatorial airglow. The volume emission rate, Q (6300), from dissociative recombination of O_2^+ and an electron may be estimated from the following relation (Peterson, VanZant and Norton, 1966; Forbes, 1970):

$$Q(6300) = \frac{A(6300)\, K_d\, \gamma [O_2]\, N_e}{A_d + s_d (N_2)\, [N_2]} \tag{2}$$

where A(6300) and A_d are Einstein Coefficients and are .0069 and .0091 sec^{-1}, respectively. $s_d (N_2)$ is the rate coefficient for quenching, γ the rate coefficient for the reaction of O^+ ion with O_2, and K_d the number of excitations per dissociative recombination. The integrated emission rate I_{6300} (zenith) may be calculated by integrating Eq. (2) for known distributions of N_e, O_2, and N_2.

$$I_{6300}\,(\text{zenith}) = 7.6 \times 10^{-7}\, K_d\, \gamma \int_0^\infty \frac{[O_2]\, N_e\, dz}{1 + 1.1 \times 10^2\, s_d (N_2)\, [N_2]} \text{ rayleighs} \tag{3}$$

Because of the strong quenching, the contribution to I_{6300} (zenith) is almost negligible below 200 km. Above this altitude, the exospheric temperature becomes nearly isothermal and O_2 and N_2 densities are in diffusive equilibrium and may be described by their scale heights. The calculated to I_{6300} (zenith) is

also very small from the altitude region above 600 km because of the sharp decrease of $[O_2]$. In the altitude region of 200-600 km we may approximate the electron density distribution by a simple Chapman function by specifying maximum electron density N_m, the height of the maximum z_m, the scale height of atomic oxygen H (O), and a shape factor S. Thus in the altitude region of 200-600 km, neglecting the height dependence of g, we may write:

$$N_e(z) = N_m \exp \frac{1}{2}\left[1 - \frac{z - z_m}{SH(O)} - \exp - \frac{(z - z_m)}{S\,H(O)}\right] \tag{4}$$

$$[O_2] = [O_2]_{z_m} \exp - \frac{(z - z_m)}{H(O_2)} \tag{5}$$

$$[N_2] = [N_2]_{z_m} \exp - \frac{(z - z_m)}{H(N_2)} \tag{6}$$

where $[O_2]_{z_m}$ and $[N_2]_{z_m}$ are the densities of O_2 and N_2 at the height of the F_2-peak and $H(O)$, $H(O_2)$ and $H(N_2)$ the scale heights of O, O_2 and N_2. From Eqs. 2-6, we may derive the expressions for I_{6300} (zenith) and the height of the maximum emission $z_{I_{max}}$ (from the condition $\partial I/\partial z = 0$).

$$I_{6300}\,(\text{zenith}) = 7.6 \times 10^{-7}\, K_d\, \gamma\, N_m\, [O_2]_{z_m}\, H(O)\, F(q(z_m), S) \tag{7}$$

$$z(I_{max}) = z_m - S\,H(O)\,\log\left(1 + 4S - 3.5\,S\,M(z_{I_{max}})\right) \tag{8}$$

where $F(q(z_m), S)$ is an integral involving the quenching term, and q (z) and M(z) are quenching parameters defined as follows:

$$F(q(z_m), S) = S\sqrt{2e}\, 2^S \int_0^\infty \frac{x^{2S-1/2} \exp - x}{1 + q(z_m)(2x)^{1.75S}}\, dx$$

$$x = \frac{1}{2} \exp - \frac{(z - z_m)}{S H(O)}$$

$$q(z) = 1.1 \times 10^2 s_d (N_2) [N_2]_z$$

$$M(z) = \frac{q(z)}{1 + q(z)}$$

The numerical values of the integral are given for the probable range of $q(z_m)$ and S in Fig. 5 and may be approximated by the following expression:

$$F(q(z_m), S) = \frac{\sqrt{2.33S} \times 2^S \Gamma(2S + 0.5)}{1 + 2^{1.75S} q(z_m) \left[A_S \frac{\Gamma(2S + 0.5)}{\Gamma(.25S + 0.5)} + \frac{B_S}{1 + q(z_m)} \right]}$$

with the values of A_S and B_S given as follows:

S	1	.9	.8	.7	.6	.5	.4	.3	.2	.1
A_S	1.21	1.20	1.20	1.20	1.20	1.21	1.22	1.24	1.26	1.28
B_S	1.71	1.41	1.55	.93	.73	.55	.40	.29	.23	.29

From Eq. (8), it is evident that the height of the maximum emission rate is always less than the height of the F_2-max. Since $M(z_{I_{max}})$ varies between 0 and 1 from no quenching to complete quenching conditions, the difference $z_m - z(I_{max})$ is a function of $z_{I_{max}}$ and varies in the range of $SH(O) \log (1 + 4S)$ and

SH(O) log (1 + 0.5S). For a typical value of S = .8 and the neutral atmosphere model (Jacchia, 1971) corresponding to T = 1300°K, we estimate z_m = 295 and 425 km, respectively corresponding to $z_{I_{max}}$ = 250 and 350 km. Thus a difference of 100 km in the height of the peak emission (Fig. 4) near the northern and the southern arc corresponds to a difference of 130 km in the heights of the F_2 -peak. Because of the geomagnetic control of ionization these differences cause a latitudinal displacement of the 6300Å arc with respect to the crest in electron density (Fig. 3).

Equation (7) shows the relative importance of the ionospheric and atmospheric parameters in determining the 6300Å emission rate. Because of the exponential relation between $O_2(z_m)$ and z_m, the changes in the height of the F_2-peak affect the emission rate much more strongly than the changes in N_m and T_n. Since T_n does not vary more than 10-20 percent in the equatorial region, the latitudinal variation in I_{6300} (zenith) is largely determined by the variations in N_m and z_m. In the African zone, the F_2 peak as inferred from Fig. 4 does not show any significant latitudinal variation. Thus N_m is the controlling parameter in determining the latitudinal characteristic and a close correspondence between the crests of the electron density and 6300Å arcs is to be expected. In the American and Asian zones, the height of the F_2 -peak in the southern latitudes is about 130-140 km higher then in the northern latitudes. With the scale height of O_2 in the range of 40-45 km, this difference in the F_2 -peak would cause the northern arc to be about 20-30 times brighter than the southern arc and would mask any variation associated with N_m. It is interesting to note that the asymmetry in the F_2 -peak only affects the 6300Å emission rate. The emission rates of 1304Å arc

relatively insensitive to the changes in the F_2-peak and are affected only by the variation in N_m^2 (Hanson, 1969).

The integrated emission rate I_{6300} (zenith) may be calculated from Eq. 7 from the measurements of N_m and z_m using a suitable atmosphere model. Unfortunately, a detailed comparison between the calculated and observed emission rates cannot be made because N_m and z_m could not be measured directly from OGO-4. We may, nevertheless, estimate their values from the measured values of $N_e(z)$ and $z_{I_{max}}$ using Eqs. (3) and (7). In the following, we present a numerical example to demonstrate the applicability of Eqs. 7 and 8 for the airglow calculations. The calculation is based on the neutral atmosphere model (Jacchia,(1971) corresponding to exospheric temperature = 1300°K. The values of γ, K_d, $s_d(N_2)$ adopted in this calculation are as follows:

$$\gamma = 3.4 \times 10^{-10}\ T^{-1/2}\ cm^3\text{-}sec^{-1} \quad \text{(Smith and Fouracre, 1968)}$$

$$s_d\ (N_2) = 7 \times 10^{-11}\ cm^3\text{-}sec^{-1} \quad \text{(Forbes 1970)}$$

$$K_d = 0.9$$

There is considerable uncertainty in the estimate of K_d. Its value has been estimated in the range of 0.1 and 1 (Forbes, 1970; Brown and Steiger, 1971) from the ionospheric measurements. We have adopted a value of 0.9 in close agreement with the laboratory measurement (Zipf, 1970).

Date: October 28, 1967

T_N = 1300°K H(O) = 80 km S = .8

OBSERVED							CALCULATED			
U.T.	Gd. Lat.	Gd. Long.	Sat. Alt.	$N_e(z)$	$z_{I_{max}}$	I_{6300} (zenith)	N_m	z_m	F(q, S)	I_{6300} (zenith)
3h 6_m	-35°	-82°	465 km	8.9×10^5/cc	350 km	75R	9.64×10^5/cc	425 km	3.6	90R
10h 59_m	25°	156°	478 km	5.3×10^5/cc	257 km	837R	1.3×10^6/cc	295 km	0.72	835R

A comparison of observed and calculated values of I_{6300} (zenith) at the stated geodetic latitudes and longitudes and satellite altitudes.

Comparing the observed and calculated values of I_{6300} (zenith), we find the agreement well within the uncertainty of the various parameters (see table). These equations, therefore, not only provide a basis for understanding the nature of the equatorial airglow but also provide useful means of estimating O_2 density from the simultaneous measurements of N_m, z_m, and I_{6300} (zenith).

The most likely cause for the asymmetry in the height of the F_2 -peak is the vertical movement associated with the neutral wind [see Rishbeth, 1972 for detailed references]. The neutral wind caused by the global pressure gradient tends to drag the ions along the geomagnetic field lines. A meridional wind blowing from south to north will tend to move the ionization upward to the south of the geomagnetic equator and downward to the north [Abur-Robb and Windle, 1969]. In this situation the F_2 -peak will be higher south of the equator resulting in the asymmetrical distribution in the airglow emission rate. The asymmetry in the height of the F_2 -peak may also produce some asymmetry in the crests of geomagnetic anomaly inferred from electron density measurements. However this asymmetry is relatively much smaller and less noticeable than the asymmetry in the 6300Å emission rate. The fact that the latitudinal asymmetry in the F_2 -peak is confined to the Asian and American zones and absent in the African zone cannot be explained in a simple way. Certain asymmetry may be ascribed to the relative orientation of the geomagnetic equator with respect to the geographic equator and the longitudinal dependence of the magnetic declination angle. But the geometrical factor alone does not seem to be sufficient to explain the longitudinal asymmetry. Any quantitative study of this problem would require a better understanding of the global pressure distribution which is the driving force for the neutral wind.

Summary and Concluding Remarks

In this paper we have presented a global picture of the equatorial airglow and have discussed some of the features which were, hitherto, undetected from the ground based measurements. Simultaneous measurements of the relevant ionospheric parameters helped in understanding the complex nature of the 6300Å emission, particularly its longitudinal asymmetry, in terms of the simple physical processes. Our study also provided a basis for estimating the O_2 density in the upper atmosphere from the simultaneous measurements of airglow emission rate and readily measurable ionospheric parameters.

We have not been able to provide an explanation for the longitudinal asymmetry in the equatorial wind system. An understanding of this problem would not only require a better comprehension of the global pressure gradients but a three-dimensional solution of the basic ionospheric and atmospheric equations. We hope that the results presented in this paper will stimulate further research in this area.

ACKNOWLEDGMENTS

We are indebted to G. T. Hicks of the Naval Research Laboratory for supplying a detailed list of the ultraviolet airglow observations and to G. Thuillier of the Centre National de la Recherche Scientifique for the derivation of the height of the 6300Å emission layer from the OPEP photometer observations.

REFERENCES

Abur-Robb, M.F.K. and D. W. Windle, On the day and night reversal in the $N_m F_2$ north south asymmetry, Planet. Space Sci., 17, 97, 1969.

Barbier, D. and J. Glaume, Les radiations de l'oxygène 6300 et 5577 Å de la luminescence du ciel nocturne dans une station de basse latitude, Ann. Géophys., 16, 319, 1960.

Barbier, D., G. Weil and J. Glaume, L'émission de la raie rouge du ceil nocturne en Afrique, Ann. Géophys., 17, 305, 1961.

Barbier, D. and J. Glaume, La couche ionospherique nocturne F dans la zone intertropicale et ses relations avec l'émission de la raie 6300 Å du ceil nocturne, Planet. Space Sci., 9, 133, 1962.

Barth, C. A. and S. Schaffner, OGO-4 spectrometer measurements of the tropical ultraviolet airglow, J. Geophys. Res., 75, 4299, 1970.

Brown, W. E. and W. R. Steiger, 6300 Å quantum efficiency of the recombination mechanism in the nighttime F-layer, Planet. Space Sci., 20, 11, 1972.

Chandra, S., B. E. Troy, Jr., J. L. Donley and R. E. Bourdeau, OGO-4 observations of ion composition and temperatures in the topside ionosphere, J. Geophys. Res., 75, 3867, 1970.

Forbes, J. M., Yield of $O(^1D)$ by dissociative recombination of O_2^+ for night airglow observations, J. Atmos. Terr. Phys., 32, 1901, 1970.

Hanson, W. B., Radiative recombination of atomic oxygen ions, J. Geophys. Res., 74, 3720, 1969.

Hicks and T. A. Chubb, Equatorial auroral airglow in the far ultraviolet, J. Geophys. Res., 75, 6233, 1970.

Jacchia, L. G., Revised static models of the thermosphere and the exosphere with empirical temperature profiles, Smithsonian Astrophysical Observatory Special Report No. 332, 1971.

King, J. W., Airglow observations and the decay of the ionospheric equatorial anomaly, J. Atmos. Terr. Phys., 30, 1968.

Knudsen, W. C., Tropical ultraviolet night glow from oxygen ion-ion neutralization, J. Geophys. Res., 75, 3862, 1970.

Olson, R. E., J. R. Peterson and J. Mosley, Oxygen ion-ion neutralization as related to tropical ultraviolet, J. Geophys. Res., 76, 2516, 1971.

Peterson, V. L., T. E. VanZandt and R. B. Norton, F-region night glow emissions of atomic oxygen, J. Geophys. Res., 71, 2255, 1966.

Reed, E. I. and J. E. Blamont, Some results concerning the principal airglow lines from the OGO-2 satellite, Space Research VII, 337, 1967.

Reed, E. I., W. B. Fowler and J. E. Blamont, An atlas of low latitude 6300 Å (OI) night airglow from OGO-4 observations, GSFC X-625-72-171, 1972.

Rishbeth, H., Theoretical winds and the F-region: A review, J. Atmos. Terr. Phys., 34, 1, 1972.

Stubbe, P. and S. Chandra, Ionospheric warming by neutral winds, Planet. Space Sci., 19, 731, 1971.

Smith, D. and R. A. Fouracre, The temperature dependence of the reaction rate coefficients of O^+ ions with molecular oxygen and nitrogen, Planet. Space Sci., 16, 243, 1968.

VanZandt, T. E. and V. L. Peterson, Detailed maps of tropical 6300 Å night glow enhancements and their implications on the ionospheric F_2 -layer, Ann. Geophys., 24, 747, 1968.

Zipf, E. C. and E. J. Stone, Photo-electron excitation of atomic oxygen resonance radiation in the terrestrial airglow, J. Geophys. Res., 76, 6865, 1971.

Zipf, E. C., The dissociative recombination of O_2^+ ions into specifically identified final atomic states, Bull. Am. Phys. Soc., 15, 418, 1970.

FIGURE CAPTIONS

Figure 1 The global map of the equatorial airglow – showing the contours of 6300 Å emission rate and the positions of the ultraviolet arc (dots) with respect to geomagnetic equator.

Figure 2 Comparison of the latitudinal characteristics of 6300 Å emission rate and ion density in the Asian, American and African zones.

Figure 3 The latitudinal variations of electron and ion temperatures (T_e and T_+) and the flux of the suprathermal electrons.

Figure 4 The distribution of the height of the maximum emission rate in the Asian, American and African zone and its relation with 6300 Å emission rate.

Figure 5 Quenching Integral $F(q_{z_m}, S)$ as a function of quenching parameter q_{z_m} and shape parameter S.

AIRGLOW 6300 Å

LOCAL TIME
2146

OCT. 26 - OCT. 30
1967

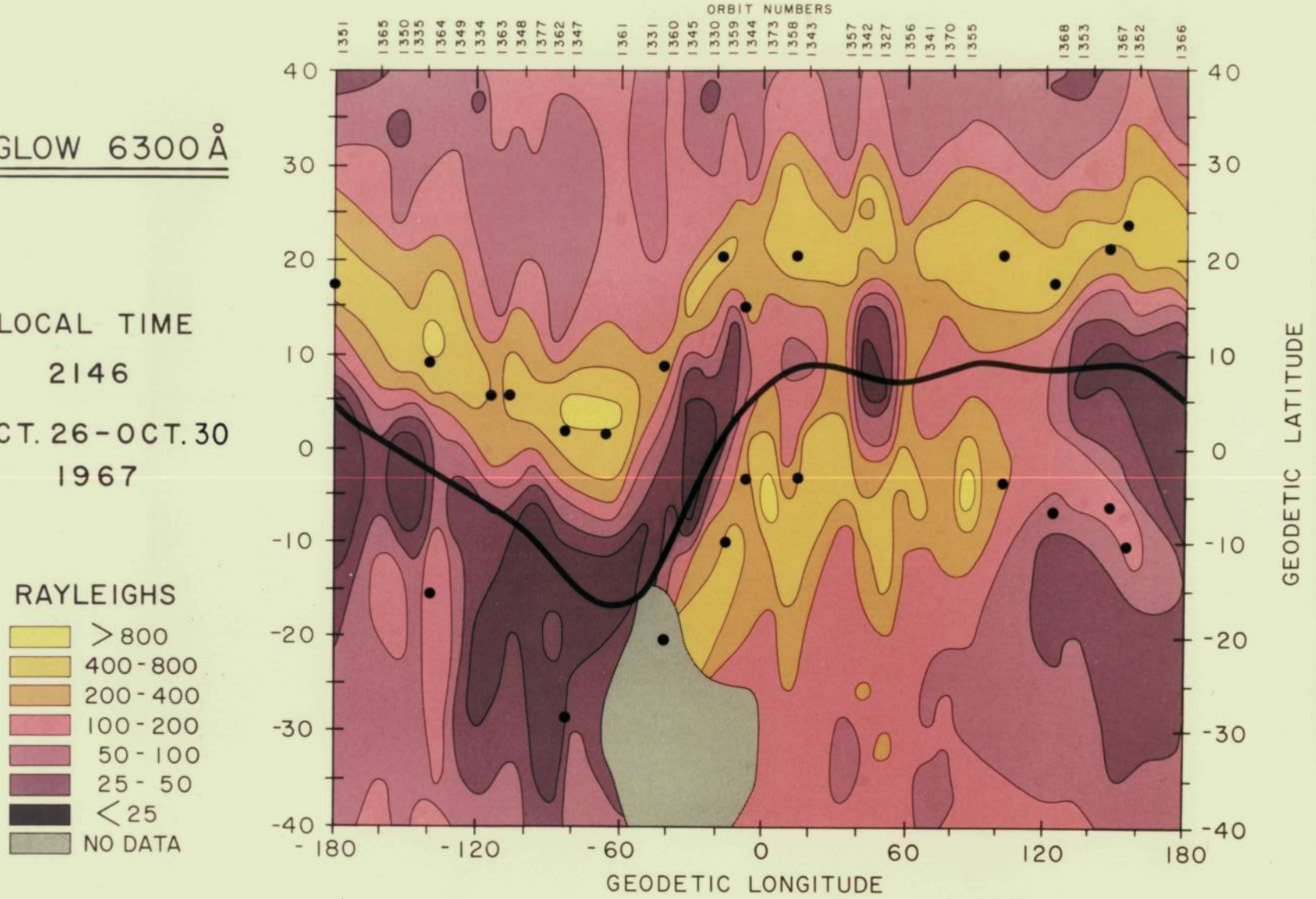

Fig 1

6300Å EMISSION RATE AND ION DENSITY VS LATITUDE

OGO–4
LOCAL TIME≃2130

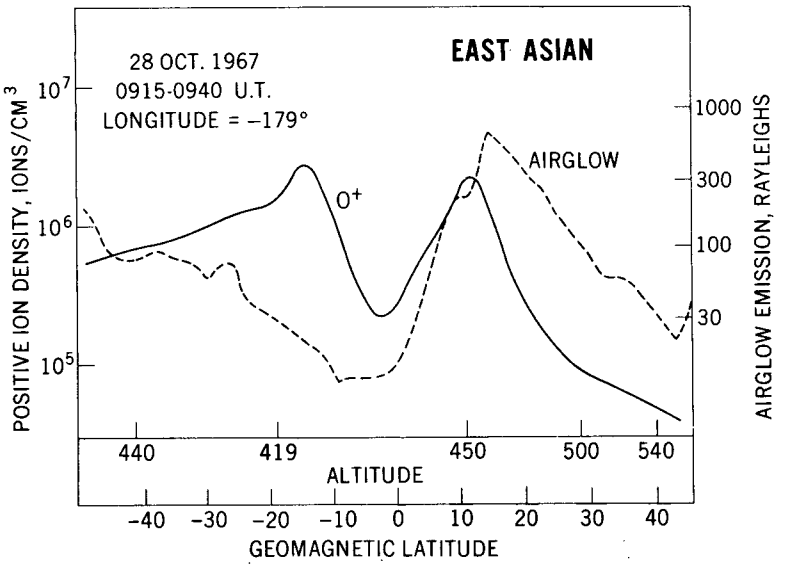

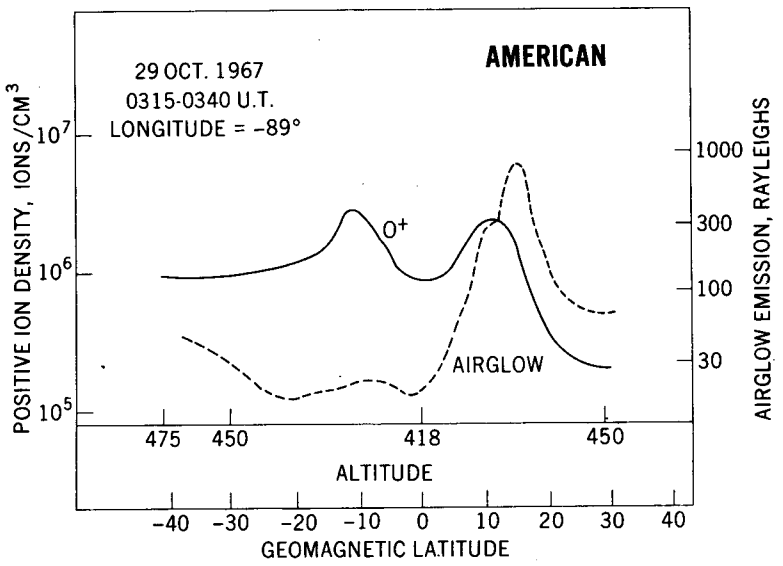

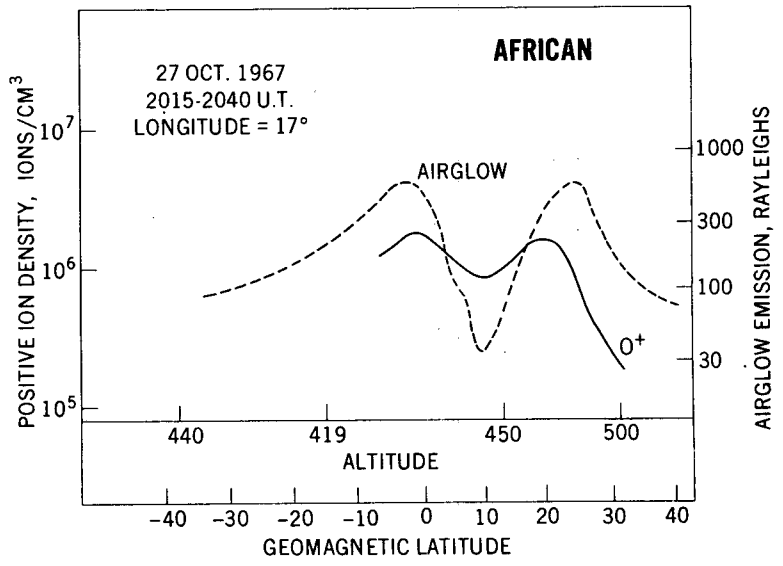

Fig. 2

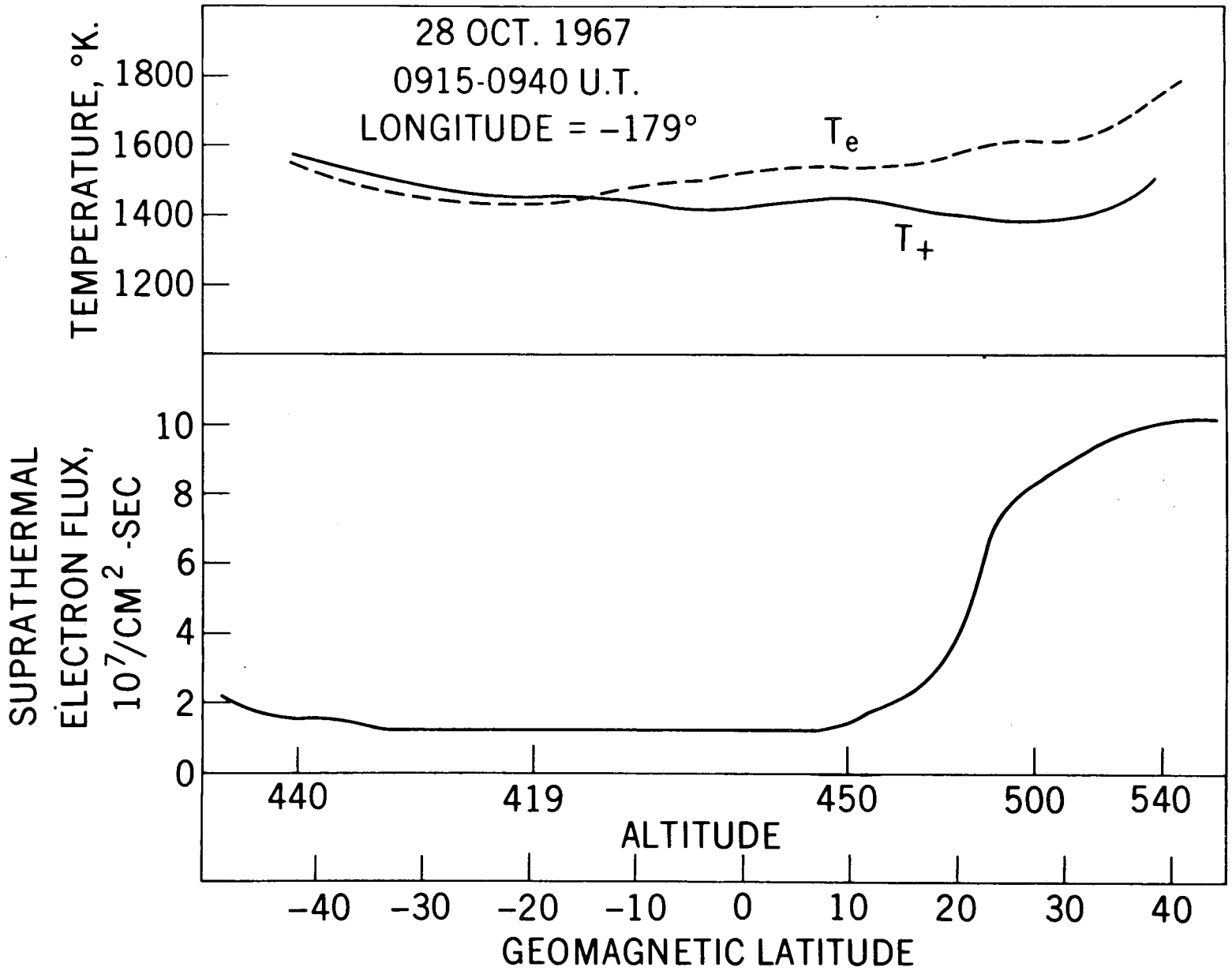
28 OCT. 1967
0915-0940 U.T.
LONGITUDE = −179°
T_e
T_+
TEMPERATURE, °K.
1800
1600
1400
1200
SUPRATHERMAL ELECTRON FLUX, $10^7/CM^2$-SEC
10
8
6
4
2
0
440
419
450
500
540
ALTITUDE
−40
−30
−20
−10
0
10
20
30
40
GEOMAGNETIC LATITUDE

Fig. 3

6300Å EMISSION RATE VS ALTITUDE OF MAXIMUM EMISSION RATE

OGO–4
OCT 22–NOV 5 1967
ABOUT 2130 LOCAL TIME

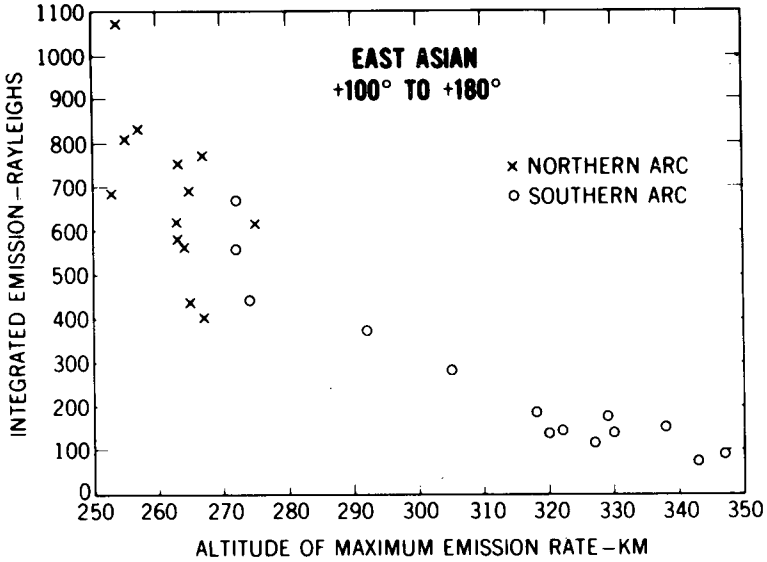

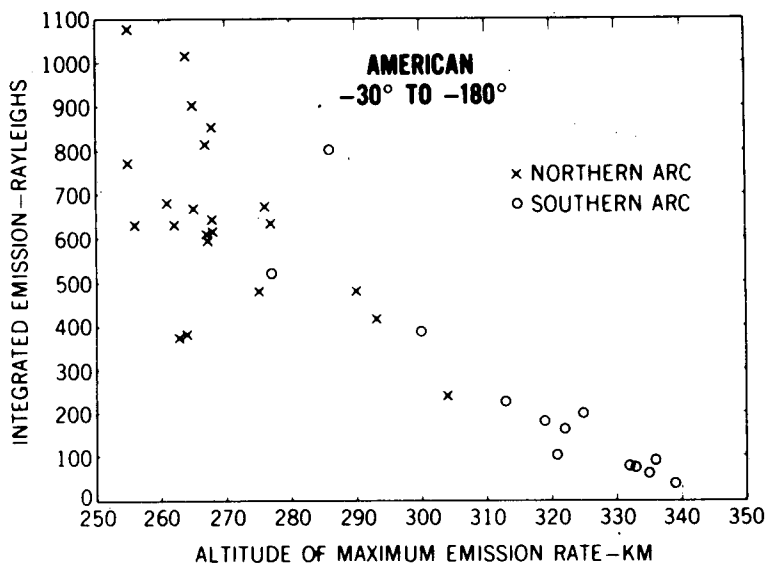

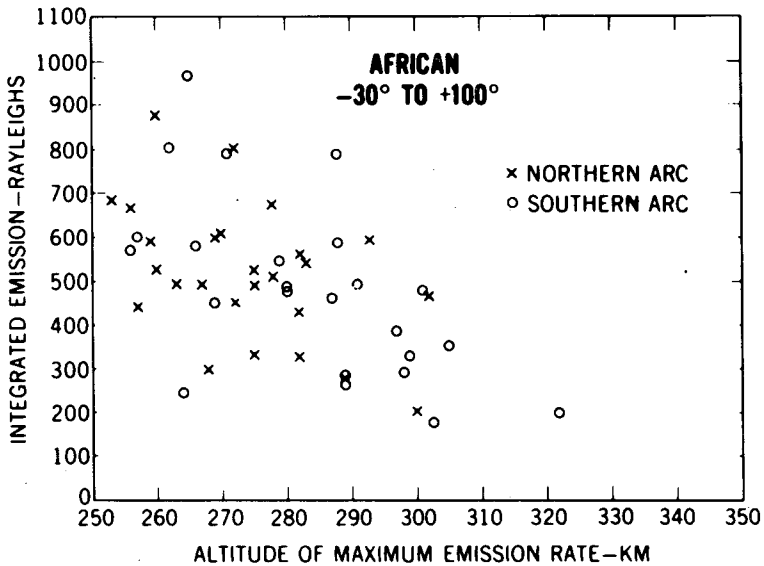

Fig. 4

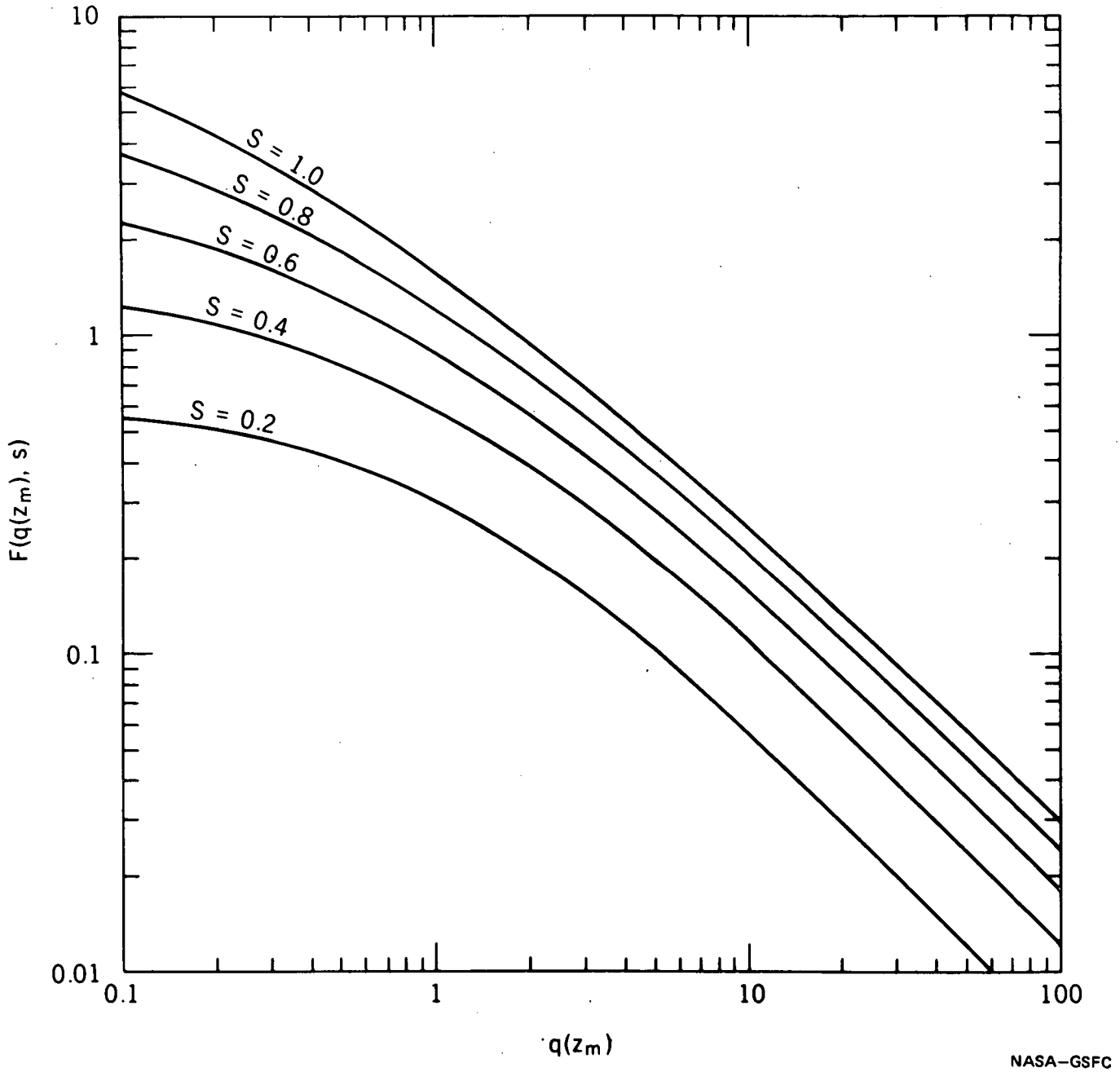

Fig. 5